Open Research Online

The Open University's repository of research publications
and other research outputs

Electronically excited states of formic acid investigated by theoretical and experimental methods

Journal Item

oro.open.ac.uk

Journal Pre-proofs

Electronically excited states of formic acid investigated by theoretical and experimental methods

P.A.S. Randi, D.F. Pastega, M.H.F. Bettega, N.C. Jones, S.V. Hoffmann, S. Eden, A. Souza Barbosa, P. Limão-Vieira

Please cite this article as: P.A.S. Randi, D.F. Pastega, M.H.F. Bettega, N.C. Jones, S.V. Hoffmann, S. Eden, A. Souza Barbosa, P. Limão-Vieira, Electronically excited states of formic acid investigated by theoretical and experimental methods, *Spectrochimica Acta Part A: Molecular and Biomolecular Spectroscopy* (2022), doi: https://doi.org/10.1016/j.saa.2022.122237

This is a PDF file of an article that has undergone enhancements after acceptance, such as the addition of a cover page and metadata, and formatting for readability, but it is not yet the definitive version of record. This version will undergo additional copyediting, typesetting and review before it is published in its final form, but we are providing this version to give early visibility of the article. Please note that, during the production process, errors may be discovered which could affect the content, and all legal disclaimers that apply to the journal pertain.

Electronically excited states of formic acid investigated by theoretical and experimental methods

P. A. S. Randi [a], D. F. Pastega [a], M. H. F. Bettega [a], N. C. Jones [b],

S. V. Hoffmann [b], S. Eden [c], A. Souza Barbosa [a,*] and P. Limão-Vieira [a,d,*]

[a] Departamento de Física, Universidade Federal do Paraná, Caixa Postal 19044, 81531-980 Curitiba, Paraná, Brazil

[b] ISA, Department of Physics and Astronomy, Aarhus University, Ny Munkegade 120, DK-8000, Aarhus C, Denmark

[c] School of Physical Sciences, The Open University, Walton Hall, Milton Keynes, MK7 6AA, UK

[d] Atomic and Molecular Collisions Laboratory, CEFITEC, Department of Physics, NOVA School of Science and Technology, Universidade NOVA de Lisboa, 2829-516 Caparica, Portugal

ABSTRACT

Absolute cross-section values are reported from high-resolution vacuum ultraviolet (VUV) photoabsorption measurements of formic acid in the photon energy range 4.7–10.8 eV (265–115 nm), together with quantum chemical calculations to provide vertical energies and oscillator strengths. The combination of experimental and theoretical methods has allowed a comprehensive assignment of the electronic transitions. The VUV spectrum reveals various vibronic features not previously reported in the literature, notably associated with $(3pa' \leftarrow 10a')$, $(3p'a' \leftarrow 10a')$, $(3sa' \leftarrow 2a'')$ and $(3pa' \leftarrow 2a'')$ Rydberg transitions. The assignment of vibrational features in the absorption bands reveal that the C=O stretching, $v'_3(a')$, the H'–O–'C deformation, $v'_5(a')$, the C–O stretching, $v'_6(a')$, and the O=C–O' deformation, $v'_7(a')$ modes are mainly active. The measured absolute photoabsorption cross sections have also been used to estimate the photolysis lifetime of HCOOH in the upper stratosphere (30–50 km), showing that solar photolysis is an important sink at altitudes above 30 km but not in the troposphere. Potential energy curves for the lowest-lying electronic excited states, as a function of the C=O coordinate, are obtained employing time dependent density functional theory (TD-DFT). These calculations have shown the relevance of internal conversion from Rydberg to valence character governing the nuclear dynamics, yielding clear evidence of the rather complex multidimensional nature of the potential energy surfaces involved.

* Corresponding authors:
E-mail address: plimaovieira@fct.unl.pt (Paulo Limão-Vieira); alessandra@fisica.ufpr.br (Alessandra Souza Barbosa).

1. Introduction

Formic acid (HCOOH) is the simplest organic acid, often used as a model molecular structure to study more complex organic systems [1], and is known to be an important pre-biotic molecule [2]. It was the first acid detected in diverse interstellar medium (ISM) environments, including in hot molecular cores (dense warm molecular condensations) [3–6], icy grain mantles [7], galactic centre clouds (~50-200 K) [6], and as a volatile product of cometary nuclei that may be used for remote sensing [5]. In such hot cores (T>100 K), formic acid gas-phase abundances are ~5×10^{-9} relative to H_2 (2×10^{23} cm^{-2}) [5]. Since gas-phase chemical reactions are not efficient in producing such complex saturated species, the relevant pathways for formic acid production in the ISM have been attributed to grain surface chemistry and subsequent mantel evaporation mechanisms [3,8]. These include initial formation on cold grain surfaces (~10 K), and once the temperature of such grains increase, upon mantle evaporation, formic acid is brought into the gas-phase [3,4]. For further details on the underlying mechanisms responsible for molecular species formation refer to Keane et al. [7] and van Dishoeck and Blake [8], and references therein. Notwithstanding, for ISM composition assessment, determination of a molecular species number density from the data recorded needs to be evaluated against wavelength-dependent absorption cross-sections. Thus, absolute values such as those provided by VUV photoabsorption measurements are needed.

Formic acid is also found within the Earth's atmosphere, occurring from both natural and anthropogenic origins. There are various industrial, agricultural and natural sources of formic acid in the Earth's atmosphere [9,10]. Natural production of formic acid within the atmosphere, include oxidation reactions of formaldehyde with water in cloud droplets, followed by outgassing [9]. Additionally, other sources include photochemical production from volatile organic compounds over forest regions [11–13], terrestrial biosphere [14,15], soils [14], ants [10], while biogenic emissions [16–18] are due to biomass burning, and anthropogenic emissions result from rural [19] and urbans/industrial areas activities [20–23] (and references therein). Once released in the atmosphere, formic acid when can last for just two to four days [9,16,22] before it is degraded by reactions with •OH radicals [19]. However, this lifetime is extended by an order of magnitude in cloudless regions of the troposphere [15,16,19,24].

Recent field measurements reveal formic acid concentrations of 100 ppt over most of the remote oceans, interrupted by large enhancements associated with continental outflow from combustion tracers and trajectory-based fire impacts [22,24]. Emissions into the atmosphere also result in an estimated 6.0 g of formic acid emitted per kg dry biomass burned from e.g., open fires in forests, savannas, crop residues and semi-fossilized peatlands [25]. Moreover,

3

biomass burning accounts for a global estimate of at least 400 Tg/y of gas-phase non-methane organic compounds [25], with formic acid contributing to ~ 60 Tg/y [15].

Various theoretical and experimental methods have been applied to investigate the molecular properties of formic acid. These include the lowest-lying ionic states by photoelectron spectroscopies [26,27], the lowest-lying neutral states by ultraviolet photoabsorption [28–37], studies of its photodissociation into OH fragments [38–43], fluorescence excitation [33,44,45], infrared and Raman spectroscopy [44,46–48], electron impact spectroscopies [49–52], and rate constants for its reactions with hydroxyl radicals [40,53]. Also relevant to the present work, theoretical methods have been applied to calculate the vertical excitation energies of the neutral molecule [54,55]. As far as ultra-violet photoabsorption is concerned, we note that previous investigations have been performed in the wavelength region from 106 nm up to 267 nm (4.6–11.7 eV) and are in general in reasonable agreement with the present cross-section values above 120 nm. Dissociative electron attachment studies of formic acid [46,56–58], report core-excited resonances at ~7.5 and 9.0 eV, which compare favourably to the parent Rydberg states in the VUV spectrum at 7.54(1) and 9.063 eV (see Sec. 5.1). Finally, we note theoretical methods have been employed to investigate the scattering of low-energy electrons by formic acid [59,60].

A literature survey reveals that some inconsistencies among the previous absolute values requires obtaining high-resolution absorption data using a facility which is established as an extremely reliable source of absolute photoabsorption cross-sections. In this joint theoretical and experimental study of formic acid, this work presents the most complete characterisation of the molecule's electronic state spectroscopy to date, over the photon energy range 4.679–10.781 eV.

Time dependent density functional theory (TDDFT/CAMB3LYP/aug-cc-pVDZ) calculations provide energies and oscillator strengths for the lowest-lying neutral states (Table 1), which are here reported for the first time either in a wider energy range or use higher level of accuracy. Additionally, potential energy curves for the lowest-lying excited states, as a function of the C=O coordinate, are also obtained from our TD-DFT method. Also, formic acid experimental absolute cross-section values (and even detailed information about its electronically excited states) can be used for modelling such chemical compounds in terrestrial and even astrophysical environments.

2. Theoretical methods

To help assigning the different features in the VUV photoabsorption spectrum, we have performed calculations on the electronic structure and properties of the electronically excited states of formic acid. The optimized ground-state geometries of the *trans-* and *cis-*conformers of formic acid (Fig. S1) have been implemented with the support of a DFT/CAMB3LYP/aug-cc-pVDZ calculation [61] in the GAMESS-US computational package [62]. In the optimized geometry, using the CCSD(T) method and the aug-cc-pVDZ basis set, a ground-state energy calculation was performed with a zero-point energy correction to determine which of the optimized conformers is most stable. It was found that the *trans-*conformer is the most stable (the relative energy, due to torsion of the OH group is 0.182 eV), and thus at room temperature its population is approximately 1000 times more abundant than the *cis-*conformer, in good agreement with Vizcaino et al. [52]. Therefore, the subsequent calculations were performed for the *trans-*conformer in the ground state optimized geometry and the discussion in the next sections are related to it only.

The vertical excitation energies and oscillator strengths of the electronically excited states of formic acid (see Table 1) were calculated employing TD-DFT [63,64] with a CAMB3LYP functional [61], and the aug-cc-pVDZ basis set as implemented in GAMESS-US [62]. We have also carried out some additional calculations with the equation of motion coupled-cluster with single and double excitations (EOM-CCSD) method [65–68], with the aug-cc-pVDZ basis set (Table S1) as implemented in Psi4 [69].

3. Experimental method

The high-resolution vacuum ultraviolet (VUV) photoabsorption spectrum of formic acid was measured in the photon energy range from 4.68 eV to 10.78 eV (Figs. 1–4) at the AU-UV beam line of the ASTRID2 synchrotron facility at Aarhus University, Denmark with assignment of the different absorption features shown in Tables 1–7. The experimental setup has been described before [70,71], so only a brief description in given here. Synchrotron radiation passes through a static gas sample filled with formic acid vapour at room temperature. The transmission windows (MgF_2) set the lower wavelength limit of detection (115 nm) with transmitted light detected by a photomultiplier tube (PMT). A capacitance manometer (Chell CDG100D) was used to measure the absolute pressure of the sample in the absorption cell. The absorption cross-sections were measured in the pressure range 0.10–1.26 mbar, as appropriate for the local cross-section, to achieve attenuations of 50% or less and hence avoid saturation effects.

5

The Beer-Lambert attenuation law, $I_t = I_0 e^{(-N\sigma l)}$, where I_t is the light intensity transmitted through the gas sample, I_o is that through the evacuated cell, N the molecular number density of formic acid, and l the absorption path length (15.5 cm), was used to obtain absolute photoabsorption cross-section values, σ, in units of megabarn ($1 \text{Mb} \equiv 10^{-18} \text{ cm}^2$). Throughout the collection of each spectrum, the synchrotron beam current was monitored, and background scans were recorded with the cell evacuated. Within the wavelength region scanned ($115 - 265$ nm), accurate cross-section values are obtained by recording the VUV spectrum in small (5 or 10 nm) sections, allowing an overlap of at least 10 points between the adjoining sections. In order to compensate for the constant beam decay in the storage ring, ASTRID2 operates in a "top-up" mode allowing the light intensity to be kept quasi-constant. The variations (2–3%) of the incident flux are therefore normalized to the beam current in the storage ring. This methodology allows us to determine photoabsorption cross-sections to an accuracy of $\pm$ 5%. The resolution in the present spectrum [70] is 0.08 nm (corresponding to 1, 3, and 7 meV at the low extreme, the midpoint, and the high extreme of the present energy range, respectively).

The liquid sample used in the VUV photoabsorption measurements was purchased from Sigma-Aldrich, with a stated purity of $\geq$ 96%. The sample was degassed through repeated freeze-pump-thaw cycles.

4. Structure and properties of formic acid

Of the *trans* and *cis* conformers of formic acid, both of C_S-symmetry in the electronic ground-state, the former is the most stable at room temperature (see Sec. 2). The calculated bond lengths (Å) and bond angles (°) for the *trans*-conformer in the electronic ground state, in low-lying neutral excited states and in the ionic electronic ground state are listed in the Supporting File (Fig. S1). The calculated outermost electronic configuration of the *trans* $\tilde{X}^1 A'$ ground state is: (a) core orbitals $(1a')^2 (2a')^2 (3a')^2$; (b) valence orbitals $(4a')^2 (5a')^2 (6a')^2 (7a')^2$ $(8a')^2 (1a'')^2 (9a')^2 (2a'')^2 (10a')^2$. The character of the ground-state MOs shows that the highest occupied molecular orbital (HOMO), 10a', is mainly the O 2p lone pair orbital $(\bar{n}_O)$ of the carbonyl group in the molecular plane. The second highest occupied molecular orbital (HOMO-1), 2a'', is $\pi(C=O)$ with the oxygen 2p orbital (n_O) of OH out of the O=C–O plane, whereas the (HOMO-2), 9a', is $\sigma(CO)$ mixed with $(\bar{n}_O)$ in the molecular plane, bonding in OH. The VUV photoabsorption features shown in Figs. 1–4 have been assigned to electronic excitations, due to the promotion of an electron from the (HOMO), (HOMO-1) and (HOMO-2) to valence,

6

Rydberg and mixed valence-Rydberg character orbitals (see Table 1 for their calculated dominant excitation energies and oscillator strengths).

The fine structure visible in the formic acid spectrum is indicative of vibronic transitions, and the present assignments are based on previously reported activation energies for vibrational modes in the electronic ground state [28–30,33,34,36,37,40]. For the valence transitions, these have been assigned based on the energies (and wavenumbers) in the ground electronic state to 0.220 eV (1777 cm^{-1}) for C=O stretching, $v_3''(a')$, 0.152 eV (1223 cm^{-1}) for H′–O–′C deformation, $v_5''(a')$, 0.077 eV (625 cm^{-1}) for O=C–O′ deformation, $v_7''(a')$, 0.128 eV (1033 cm^{-1}) for CH deformation, $v_8''(a'')$, and 0.080 eV (642 cm^{-1}) for OH deformation, $v_9''(a'')$. Additionally, for the Rydberg character of the electronic transitions, the main vibrational modes have been assigned according to the experimental information from He(I) photoelectron spectroscopy [26,27] to 0.185 eV (1 ^{2}A′) and 0.291 eV (1 ^{2}A″) for $v_3'(a')$, 0.148 eV (1 ^{2}A′) and 0.164 eV (1 ^{2}A″) for $v_5'(a')$, 0.148 eV (1 ^{2}A′) and 0.128 eV (1 ^{2}A″) for $v_6'(a')$ and 0.063 eV (1 ^{2}A′) and 0.071 eV (1 ^{2}A″) for $v_7'(a')$.

The assignment of the different Rydberg orbitals based on their quantum defects, is obtained for the two lowest experimental adiabatic ionisation energies taken from the He(I) photoelectron data of Leach et al. [26] to be 11.3246 eV $(10a')^{-1}$ and 12.3783 eV $(2a'')^{-1}$.

5. Results and discussion

The absorption spectrum of HCOOH reported by Leach et al. [33] was recorded above 6 eV, where our data appears in some photon energy sections better resolved meaning that the magnitude of the cross-sections for these are higher relative to this earlier work [33]. Fig. 1 shows the present absolute photoabsorption spectrum of formic acid in the energy range 4.679 to 10.781 eV, while expanded views of the spectrum are in Figs. 2–4. The major absorption bands can be classified as originating from valence, Rydberg and a mixture of valence-Rydberg excitations (see Section 5.4) converging to the ionic electronic ground state $(10a')^{-1}$, and the ionic first electronic excited state $(2a'')^{-1}$. The spectrum shows extensive fine structure, with the C=O stretching, $v_3'(a')$ and O=C–O′ deformation, $v_7'(a')$ modes dominant in the energy range 4.5–7.0 eV. At higher energies the H′–O–′C deformation, $v_5'(a')$, CH deformation, $v_8'(a'')$, and OH′ deformation, $v_9'(a'')$ modes also contribute. The structure above 8.7 eV is largely due to the overlap of different Rydberg transitions contributing to the spectrum. Table 1 shows the TD-DFT calculation results for the *trans*-conformer of formic acid alongside the experimental data, and a reasonably good level of agreement is noted. The assignments for fine structure

7

associated with the Rydberg transitions have not been labelled in Fig. 4 in order to avoid congestion. Tables 6 and 7 list these vibronic assignments and compare them with previous work wherever possible.

Formic acid photoabsorption bands in Fig. 1 are assigned to the $\pi_{CO}^*(3a'')\leftarrow\bar{n}_O(10a')$, $\left(3sa'(11a')\leftarrow\bar{n}_O(10a') + \pi^*(3a'')\leftarrow\pi(2a'')\right)$, $\left(\pi^*(3a'')\leftarrow\pi_{CO}(2a'')\right)$, $\left(nsa',npa',np'a',nda'\leftarrow\bar{n}_O(10a')\right)$ and $\left(nsa',npa',npa'',nda''\leftarrow(n_O)\right)$ transitions. A detailed description of the VUV photoabsorption features, in the different photon energy ranges, are presented and discussed together with the aid of our theoretical calculations, in the next sections.

5.1. The 4.5–7.0 eV photon energy range

The lowest-lying singlet-singlet valence transition, is assigned to promotion of the oxygen lone pair orbital of the carbonyl group in the molecular plane, $(\bar{n}_O)$, to a π^* molecular orbital, $\pi_{CO}^*(3a'')\leftarrow\bar{n}_O(10a'), \left(1^1A''\leftarrow\tilde{X}^1A'\right)$, with a local cross-section of 0.19 Mb. The rather low-intensity of the absorption band is due to the type of electronic transition, from the A′ ground state to the upper excited A″ state, which is polarised normal to the plane of the molecule [72]. The vertical excitation energy value of 5.910 eV is in good agreement with the calculated value 5.767 eV as shown in Table 1. This band has been reported before [35,37,38,43,54], with intensities in good accord with the present experiment; we calculated an oscillator strength of $f_L \approx 0.001$ while Demoulin [54] reported $f_L \approx 0.014$ and Basch et al. [35] reported $f_L \approx 0.007$. Moreover, the oscillator strength value obtained at the EOM-CCSD level of theory (see Table S1) is also in good accord with the TD-DFT calculation result, and a rather higher calculated energy than the experimental value. Note that the magnitude of the present low-lying absorption band in the 220–260 nm wavelength region (4.768–5.636 eV) recorded at ~1.3 mbar, is in excellent agreement with Ebata et al.'s [38] absorption spectrum obtained at 10 Torr (7.5 mbar).

Fig. 2 reveals the fine structure due to vibronic excitation in the 4.5–7.0 eV energy region in greater detail than any previous measurements. The origin of the band has been identified at 4.641 eV [55] from laser induced fluorescence experiments, the 0_0^0 transition is not observed in the present work. This band also shows a contribution of a 3_0^n (n = 1–15) progression from the C=O stretching, $v_3'(a')$, with an average spacing of 0.123 eV (992 cm^{-1}), together with contributions from the O=C–O′ deformation, $v_7'(a')$ mode (see Table 2a). A close inspection of the absorption band reveals that it is also dominated by extended vibrational progressions involving the C=O stretching mode, $v_3'(a')$, where the average excitation energy is 0.121 eV,

together with a few quanta of the OH deformation mode, $v_9'(a'')$ (Table 2b). Another interesting aspect pertains to the lengthening of the C=O bond, from 1.200 Å in $\tilde{X}\,^1A'$ to 1.319 Å in the 1 $^1A''$ state (Fig. S1), and consequently a decrease in the C=O stretching frequency, $v_3'(a')$, (1777 cm^{-1} in $\tilde{X}\,^1A'$) [44]. This is consistent with the previous work of Ng and Bell [30]. Moreover, in the $\left(1\,^1A''\leftarrow\tilde{X}^1A'\right)$ transition, the O=C–O′ bond angle changes from 124.7° to 109.8° (Fig. S1) and the O=C–O′ deformation mode, $v_7'(a')$, decreases from 625 cm^{-1} (0.077 eV) to 379 cm^{-1} (0.047 eV) (Table 2a). Such behaviour is consistent with the geometry change of the 1 $^1A''$ state (Fig. S1) where both H atoms are twisted out-of-plane lending evidence for the OH′ deformation mode, $v_9'(a'')$, decrease from 642 cm^{-1} (0.080 eV) to 395 cm^{-1} (0.034 eV) (Table 2a).

A detailed analysis of Fig. 2 reveals a change in the slope of the band around 5 eV. This may suggest the presence of another state contributing to the absorption characteristic. Demoulin [54], Basch et al. [35], Iwata and Morokuma [73] and Randi et al. [60] respectively calculated excitation energies of 4.60, 6.27 and 5.13eV, and 5.708 eV for the $^3(\pi^*\leftarrow n_O)$, $\left(^3A''\leftarrow\tilde{X}^1A'\right)$ transition. The present calculations yield a vertical energy of 5.81 eV for the transition. While such optically forbidden transitions are typically indiscernible in experimental absorption spectra, the rather low-intensity of the absorption band (< 0.2 Mb) may also be related in some way to such underlying contribution.

Finally, 222 nm (5.585 eV) photodissociation dynamics studies from Irwin et al. [40], Jolly et al. [39] and Singleton et al. [43], have shown that C–OH bond excision dominates, with reported quantum yields of φ_{OH}(HCOOH) ranging from 0.7 to 1.0 at 298 K.

5.2. The 7.0–9.4 eV photon energy range

This energy range comprises a broad structureless feature centred at 7.51(4) eV, which is assigned to a mixed valence-Rydberg $\left(3sa'(11a')\leftarrow\bar{n}_O(10a') + \pi^*(3a'')\leftarrow\pi(2a'')\right)$, $\left(2^1A'\leftarrow\tilde{X}^1A'\right)$ transition with a cross-section of 5.22 Mb. This band has been reported by Leach et al. [33] at 7.533 eV and its valence character has been assigned to $\left(\pi^*\leftarrow\sigma_{CO}\right)$. Yet, the present calculations show the electron spin densities of the valence MOs to be reminiscent of π character (Fig. S2). Another relevant aspect from a careful inspection of Leach et al.´s [33] data to the present work, reveals differences in shape and magnitude across the entire band. Other investigations reported this band with the maximum cross-section centred at ~155 nm (7.514 eV) [28] and 7.798 eV [31], but the latter with an intensity higher than that of the present

9

experiment. Furthermore, the oscillator strength value obtained at the EOM-CCSD level of theory (see Table S1) is also in good accord with the TD-DFT calculation result (Table 1), although with a rather higher calculated energy than the corresponding experimental value. A close comparison of the absorption features between 7.999 eV and 8.670 eV (Fig. 3) with the jet-cooled formic acid beam absorption pattern from Mualem et al. [32] and Barnes and Simpson [36] in the energy region 6.819–9.299 eV, shows no resemblance, meaning that the present room temperature spectrum contains no evidence for dimers.

The calculated electronic transition at 8.066 eV, with an oscillator strength $f_L \approx 0.05$, i.e. 60% higher than the value for the previous $\left(2^1 A' \leftarrow \tilde{X}^1 A'\right)$ transition (Table 1), is tentatively assigned to $3s(15a'/12a') \leftarrow \bar{n}_O(10a')$, $\left(3^1 A' \leftarrow \tilde{X}^1 A'\right)$ from the shape of the MOs (Fig. S2), and has no correspondence with any discernible experimental feature in the photoabsorption spectrum (Fig. 3). Regardless the different basis set (aug-cc-pVDZ and aug-cc-pVTZ not show here) we have used to calculate the nature of such transition, these have led to the conclusion that it is Rydberg in character with a quantum defect $\delta = 0.96$ characteristic of a 3s transition. However, if we take the next absorption feature at 8.109 eV, a quantum defect $\delta = 0.94$ is obtained, although this feature has been assigned to belong to a valence transition with a progression of the C=O stretching mode, $v_3'(a')$ (see below).

The next electronic transition, with the 0_0^0 origin at 8.109 eV, is assigned to $\pi^*(3a'') \leftarrow \pi_{C=O}(2a'')$, $\left(4^1 A' \leftarrow \tilde{X}^1 A'\right)$ although with some Rydberg character (Sec. 5.4). It is worth noting that the calculations in Table 1 show that the dominant excitations are due to 11a' ← 10a' (5.1%), 13a' ← 10a' (14.1 %) and 3a'' ← 2a'' (68.1 %). The vertical excitation energy of 8.285 eV is in fair agreement with the theoretical value of 8.573 eV from the present calculations (Table 1). This band has been reported before [28,29,33,34,36] with a maximum cross-section of 35.13 Mb, slightly higher than previous experiments [28,33]. The transition's calculated oscillator strength $f_L \approx 0.15$ is in good accord with Leach et al.'s [33] and Basch et al.'s [35] value of $\approx$ 0.2. However, the latter authors predict an energy of 12.023 eV for this transition which is certainly much higher than the calculated value. This band also shows a contribution of a 3_0^n (n = 1–6) progression of the C=O stretching mode, $v_3'(a')$, with an average spacing of 0.182 eV (1468 cm^{-1}), together with contributions (one quantum) from the O=C–O' deformation and H'–O–'C deformation modes, $v_7'(a')$ and $v_5'(a')$ (see Table 3). Note that in Fig. 3 we have marked 3_0^4 to 3_0^6 as dashed lines, since the corresponding features appear in the spectrum with weaker intensities relative to the first three quanta of such C=O stretching mode excitation. To support the assignments of these new features, we have performed quantum chemical calculations

10

within the photon energy region conveying the contribution of the $n = 4$ member of the nsa′ Rydberg series (see Table 5). The calculations in Fig. S1 show lengthening of the C=O bond, from 1.200 Å in X̃ $^1A'$ to 1.261 Å in the 8 $^1A'$ state, and consequently a modest decrease in the C=O stretching frequency, $v'_3(a')$. Moreover, potential energy curves have been obtained along the C=O reaction coordinate to investigate the nature of the nuclear dynamics in the energy region where the 3^n_0 ($n = 1$–6) progression from the C=O stretching mode, $v'_3(a')$ has been assigned (see Sec. 5.5). The calculations show a relevant internal conversion from the initial Rydberg transition to a valence character within the adiabatic description as the C=O bond is stretched. This lends strong support to weakening of the bond and the activation of C=O stretching vibration within the potential energy well (see Figs. S3 and S4).

5.3. The 8.7–10.8 eV photon energy range

The absorption features in this photon energy region are classified as valence and Rydberg (Sec. 5.4) and have been reported before [28,29,33–36] with extensive vibrational fine structure (Tables 4, 6 and 7). An expanded plot of the current measured photoabsorption spectrum is presented in Fig. 4, with our proposed assignments summarised in Tables 1, 4 – 7. Note that several of the features' energy positions are superimposed either on the vibrational progressions or on the Rydberg series, thus broadening the shape of some peaks. The two discernible valence excited states have 0^0_0 transitions at 8.923 and 8.952 eV, with cross-sections of 28.43 and 35.97 Mb, while Leach et al. [33] have reported their origins at 8.919 and 8.95 eV. From the calculations in Table 1, these features have been assigned to the $\left(\pi^* \leftarrow \pi_{C=O}(2a'')\right)$ $\left(4^1A'' \leftarrow \tilde{X}^1A'\right)$ and the $\left(\sigma^* \leftarrow \bar{n}_O(10a')\right)$ $\left(5^1A' \leftarrow \tilde{X}^1A'\right)$ transitions, with oscillator strengths of 0.002 and 0.098, and they show relevant fine structure superimposed on a diffuse background. The absorption bands appear to be superimposed on an underlying absorption continuum that may be attributed to pre-dissociation. The transitions are accompanied by 3^n_0 progressions (for the former, $n = 1$–5; for the latter, $n = 1$–3) from the C=O stretching mode, $v'_3(a')$, with an average spacing of 0.171 eV (1379 cm^{-1}), together with contributions from the C–O stretching, $v'_6(a')$ and O=C–O′ deformation, $v'_7(a')$, modes (see Table 4), with average spacings of 0.091 eV (734 cm^{-1}) and 0.066 eV (532 cm^{-1}), respectively. These activation energies are lower than the ground-state equivalents, providing evidence of lengthening of the C=O and C–O bonds as well as a possible lack of planarity of these upper excited states.

This energy range, the photoabsorption spectrum also includes features due to the contribution of members of the different Rydberg series converging to the ionic electronic

11

ground $(10a')^{-1}$ and first $(2a'')^{-1}$ excited states of formic acid (Section 5.4), and associated vibronic structure, as discussed in the section below.

5.4. Rydberg transitions

This section addresses Rydberg transitions converging to the ionic electronic ground state $(10a')^{-1}$ and ionic first electronic excited $(2a'')^{-1}$ state of formic acid. The Rydberg character of the absorption features in the spectrum is prominently observed above 7.5 eV, where transitions to the $^1A''$ state are expected to be much weaker than to $^1A'$ state. However, due to the rich fine structure found in the photon energy region from 7.5 to 10.8 eV (Fig. 1), most of the vibronic transitions appear particularly enhanced. The present experimental energies, proposed assignments and quantum defects are listed in Table 5. For each absorption feature energy position, we have used the well-known Rydberg formula: $E_n = IE - \frac{R}{(n - \delta)^2}$, where IE is the ionisation energy of a given MO, n is the principal quantum number of the Rydberg orbital of energy E_n, R is the Rydberg constant (13.61 eV), and δ is the quantum defect resulting from the penetration of the Rydberg orbital into the core. Previous works have provided Rydberg assignments in the formic acid VUV spectrum [28,29,33–36], while Leach et al. [33] have also reported vibrational modes contributing to the spectrum. However, the present assignments on the fine structure superimposed on the Rydberg transitions up to 10.8 eV, represent to the most complete analysis to date and include various assigned features which have not been reported before (Tables 6 and 7).

The lowest-lying Rydberg transition converging to the ionic electronic ground-state, $(10a')^{-1}$, is assigned to the $(3sa' \leftarrow 10a')$ excitation, with the first member ($n = 3$) at 7.51(4) eV and having a quantum defect $\delta = 1.11$. The quantum defect is slightly larger than is typically expected for a ns series, and this can be attributed to a mixed valence-Rydberg character of this electronic transition (see Sec. 5.2). Following the discussion in Sec. 5.2, we also assign $3sa'$ at 8.109 eV. This result is in good agreement with the 8.105 eV value reported by Leach et al. [33] (Table 5) and by Bell et al. [34]. Other higher-order Rydberg members of the nsa' series, the $n = 4$ and 5, are also reported in Table 5.

The first members of the two np $(npa' \leftarrow 10a')$ and $(np'a' \leftarrow 10a')$ series are associated with absorption features at 8.843 eV and 9.063 eV ($\delta = 0.66$ and 0.55) (Table 5). Corresponding results from Leach et al. [33] have given values of 8.839 and 9.059 eV. Note that we were able to assign for the first time a $(5p'a' \leftarrow 10a')$ transition at 10.661 eV with a quantum defect $\delta = 0.47$. Table 5 also includes one nd $(nda' \leftarrow 10a')$ series (n = 3–5), where the n = 3 feature has

been assigned at 9.656 eV ($\delta = 0.14$). Other transitions to the nda' Rydberg members, $n = 4$ and 5, are also discernible.

The Rydberg series converging to the ionic electronic first excited state, $(2a'')^{-1}$, are listed in Table 5, and have been assigned to the $(nsa', npa', npa'', nda'' \leftarrow 2a'')$ transitions. The first members of these series ($n = 3$) are associated with features at 8.958 eV ($\delta = 1.00$), 9.770 eV ($\delta = 0.72$), 9.947 eV ($\delta = 0.63$) and 10.725 eV ($\delta = 0.13$) (Table 5). We note that Leach et al. [33] reported slightly lower energy values than the present absolute photoabsorption data. Assignments for higher lying members ($n > 3$) of these Rydberg series have not been attempted because they lie outside the photon energy range investigated.

The absorption spectrum around the Rydberg excitations is rich in fine structure from the different vibronic transitions (Tables 6 and 7). As noted in Sec. 2, we will make use of the information available from the He(I) photoelectron data [26] on the vibrational frequencies for the (1 ^{2}A$'$) and (1 ^{2}A$''$) states of formic acid cation. Table 6 contains the assignments for the fine structure of the Rydberg series converging to the ionic electronic ground state $(10a')^{-1}$. The most representative contributions are from the C=O stretching, $v'_3(a')$, the H$'$–O–$'$C deformation, $v'_5(a')$, the C–O stretching, $v'_6(a')$, and the O=C–O$'$ deformation, $v'_7(a')$ modes. Some of the energies of those transitions were previously reported by Leach et al. [26], some discrepancies are observed here between the present investigation and that earlier study, while several others are reported here for the first time. Interesting to note that we find in Table 6 progressions in v'_3, v'_5, and v'_7 with average frequencies diminished to 1443 cm^{-1} (0.179 eV) (1495 cm^{-1} in 1 ^{2}A$'$), 1178 cm^{-1} (0.146 eV) (1196 cm^{-1} in 1 ^{2}A$'$) and 476 cm^{-1} (0.059 eV) (510 cm^{-1} in 1 ^{2}A$'$), with respect to their values in the neutral ground state, 1777 cm^{-1} (0.220 eV), 1223 cm^{-1} (0.152 eV) and 625 cm^{-1} (0.077 eV), respectively. Furthermore, progressions in v'_6 frequency are slightly increased to an average value of 1186 cm^{-1} (0.147 eV) (1196 cm^{-1} in 1 ^{2}A$'$) compared with the neutral ground state value of 1104 cm^{-1} (0.137 eV). These variations are related to changes in geometry in the excited states (Fig. S1). The assignments of the vibrational features associated with the ($4sa' \leftarrow 10a'$), ($4pa' \leftarrow 10a'$) and ($5sa' \leftarrow 10a'$), that involve progressions in v'_5 and v'_6 have been labelled $5^1_0/6^1_0$, due to similar values of their activation energies in the 1 ^{2}A$'$ state from the He(I) photoelectron spectrum [26].

An inspection of Table 7 for the vibronic assignments of the Rydberg series converging to the ionic electronic first excited state $(2a'')^{-1}$ reveals that progressions in v'_3 and v'_5, with average frequencies increased to 2025 cm^{-1} (0.251 eV) (2343 cm^{-1} in 1 ^{2}A$''$) and 1210 cm^{-1} (0.150 eV) (1324 cm^{-1} in 1 ^{2}A$''$), with respect to their values in the neutral ground state, while progressions

13

in v_6' frequency are increased to an average value of 879 cm^{-1} (0.109 eV) (1029 cm^{-1} in 1 ^{2}A″) with respect to the neutral ground state. These changes can also be attributed to the differences found in the geometries of the excited states relative to the neutral ground-state.

5.5. Potential energy curves along the C=O coordinate

We have performed calculations of the potential energy curves (PECs) along the C=O coordinate, at the TDDFT/CAMB3LYP/aug-cc-pVDZ level of theory in the C_1 symmetry group. The nine lowest-lying excited states and their characters are presented in Figs. 5 and S2. A close inspection of the PECs in Fig. 5 shows some avoided crossings, implying that in the adiabatic description as the bond is stretched, the initial Rydberg character can change to valence character. The first excited state, $\pi_{CO}^*(3a'') \leftarrow \bar{n}_O(10a')$, shows a bound character up to $R_{C=O} = 1a_0$ (Fig. S3), which is consistent with the structure in the 4.5–7.0 eV energy region of the VUV photoabsorption spectrum. The higher energy states (labelled in Fig. 5 as 6, 7, 8 and 9) are almost degenerate at $R_{C=O}$ equilibrium distance, which is not surprising given that they originate from the same MOs, i.e., either the HOMO (($\bar{n}_O$10a′)) or the HOMO-1 ($\pi_{C=O}$(2a″)). However, states 6 and 7, at about 9.0 eV, cross slightly above the equilibrium internuclear distance (~0.025a_0). This results in a relevant adiabatic character, which can be responsible for the internal conversion from an initial Rydberg character of the transition to a valence dissociative state in the asymptotic limit, as $R_{C=O}$ is stretched away from its equilibrium distance. In this transition, such dynamical behaviour may be responsible for the quite long 3_0^n ($n = 1$–6) progression from the C=O stretching mode, $v_3'(a')$ (Sec. 5.2). However, we also note that states 8 and 9 (~9.25 eV) cross at the $R_{C=O}$ equilibrium distance where avoided crossings in the Franck-Condon region can certainly take the system through state 6 which leads to a valence character along the C=O stretching coordinate. It is worth mentioning that the different avoided crossings observed for states 6–9 may imply therefore multiple conical intersections in the full multi-dimensional space. This is outside the scope of the present work, but may be relevant to investigate by other research groups to obtain information about the complex dynamics of the underlying formic acid molecular mechanisms that yield internal conversion and/or dissociation.

5.6. Absolute photoabsorption cross sections and atmospheric photolysis

The previous absolute ultra-violet photoabsorption studies of formic acid cover the ranges 56 – 207 nm (6–22 eV) [33], 95 – 138 nm (9–13 eV) [42], 110 – 180 nm (6.888–11.271 eV) [34], 110 – 200 nm (11.271–6.199 eV) [29], 111 – 286 nm (4.340–11.159 eV) [36], 150 – 190

14

nm (6.525–8.266 eV) [31], 195 – 250 nm (4.959–6.358 eV) [37], and 200 – 267 nm (6.199–4.644 eV) [30], are found, generally speaking, in reasonable agreement with the present cross-sections to within around 10%, except for Price and Evans [29], Ng and Bell [30], Mualem et al. [32] and Bell and co-workers [34] who do not report absolute values.

We have assessed the atmospheric photolysis of formic acid from sea level up to the stratopause (50 km altitude) using the present high-resolution VUV absolute photoabsorption cross sections and NASA solar actinic flux data [74]. Details of the methodology can be found from the work of Limão-Vieira and co-workers [75]. The quantum yield for dissociation is taken to be 0.7 for C–OH bond excision, from the work of Irwin et al. [40] and Singleton et al. [43]. Photolysis lifetimes of less than 10 sunlit days were calculated at altitudes above 30 km. However, at lower altitudes (< 25 km) the photolysis lifetimes of formic acid are high (> 100 sunlit days). Singleton et al. [53] reported a gas-phase kinetics study for the HCOOH + OH reaction, finding rate values of k_{OH} (297 K) = 4.5×10^{-13} cm^3 molecule^{-1} s^{-1} in good agreement with the temperature-independent rate coefficient of $(4.62 \pm 1.16) \times 10^{-13}$ cm^3 molecule^{-1} s^{-1} from Wine and co-workers [76]. According to Puxbaum et al. [24], the reaction of formic acid with •OH radicals yields an estimated atmospheric lifetime of 25 days which is consistent with the model calculation of Yuan et al. [23]. Hence, the present assessment supports the previous understanding that reactions with •OH radicals dominate formic acid removal the troposphere. By contrast, our results demonstrate that UV photolysis is a key removal process of any formic acid in the stratosphere.

6. Conclusions

We have measured a high-resolution VUV spectrum of formic acid over the photon energy range between 4.679–10.781 eV (265–115 nm). This work provides a comprehensive study of the VUV electronic spectroscopy of the molecule, and it also provides the most reliable set of absolute photoabsorption cross-sections in the photon energy range investigated. The features in the spectrum have been assigned to valence, Rydberg and mixed valence-Rydberg transitions with the help of quantum chemical calculations, on the vertical excitation energies and oscillator strengths.

The analysis of fine structure in the photoabsorption spectrum has enabled various new assignments to be made for vibronic features the C=O stretching, $v'_3(a')$, the H′–O–′C deformation, $v'_5(a')$ and the C–O stretching, $v'_6(a')$ modes. The absolute photoabsorption cross-sections have also been used to derive photolysis rates in the terrestrial atmosphere from the surface up to the limit of the stratosphere, indicating that solar photolysis is expected to be a

15

key sink for formic acid at altitudes higher than 30 km. Potential energy curves as a function of the C=O coordinate, for the nine lowest-lying excited states, were calculated at the TD-DFT level of theory with aug-cc-pVDZ basis set. These have provided new insights into the excited state dynamics as the reaction coordinate is stretched, with important avoided crossings responsible for internal conversion from initial Rydberg states to final valence character.

Declaration of Competing Interest

The authors declare that they have no known competing financial interests or personal relationships that could have appeared to influence the work reported in this paper.

Data availability

Data presented in this publication are available upon request to the authors.

Appendix A. Supplementary material

See the supplementary material for the ground-state *trans*-conformer, first excited state, 4s Rydberg state and ionic ground state geometries, the shape of a selection of formic acid's molecular orbitals, potential energy curves of the formic acid nine lowest excited states, as a function of the $R_{C=O}$ coordinate.

ORCID

P. A. S. Randi: 0000-0002-5617-5163

A. Souza Barbosa: 0000-0001-7989-1878

N. C. Jones: 0000-0002-4081-6405

S. V. Hoffmann: 0000-0002-8018-5433

S. P. Eden: 0000-0001-7065-6222

M. H. F. Bettega: 0000-0001-9322-1360

P. Limão-Vieira: 0000-0003-2696-1152

References:

[1] G.A. Kumar, Y. Pan, C.J. Smallwood, M.A. McAllister, Low-barrier hydrogen bonds: Ab initio and DFT investigation, J. Comput. Chem. 19 (1998) 1345–1352.

[2] S. Becker, I. Thoma, A. Deutsch, T. Gehrke, P. Mayer, H. Zipse, T. Carell, A high-yielding, strictly regioselective prebiotic purine nucleoside formation pathway, Science (80-.). 352 (2016) 833–836.

[3] S. Liu, D.M. Mehringer, L.E. Snyder, Observations of Formic Acid in Hot Molecular Cores, Astrophys. J. 552 (2001) 654–663.

[4] S. Liu, J.M. Girart, A. Remijan, L.E. Snyder, Formic Acid in Orion KL from 1 Millimeter Observations with the Berkeley-Illinois-Maryland Association Array, Astrophys. J. 576 (2002) 255–263.

[5] D. Bockelée-Morvan, D.C. Lis, J.E. Wink, D. Despois, J. Crovisier, R. Bachiller, D.J. Benford, N.Biver, P. Colom, J.K. Davies, E. Gérard, B. Germain, M. Houde, D. Mehringer, R. Moreno, G. Paubert, T.G. Phillips, H. Rauer, New molecules found in comet C / 1995 O1 (Hale-Bopp) Investigating the link between cometary and interstellar material, Astron. Astrophys. 353 (2000) 1101–1114.

[6] M.A. Requena-Torres, J. Martín-Pintado, A. Rodríguez-Franco, S. Martín, N.J. Rodríguez-Fernández, P. De Vicente, Organic molecules in the Galactic center Hot core chemistry without hot cores, Astron. Astrophys. 455 (2006) 971–985.

[7] J. V. Keane, A.G. G.M.Tielens, A.C.A. Boogert, W.A.Schutte, D.C.B. Whittet, Ice absorption features in the 5–8 μm region toward embedded protostars, Astron. Astrophys. 376 (2001) 254–270.

[8] E.F. van Dishoeck, G.A. Blake, Chemical Evolution of Star-Forming Regions, Annu. Rev. Astron. Astrophys. 36 (1998) 317–368.

[9] B. Franco, T. Blumenstock, C. Cho, L. Clarisse, C. Clerbaux, P.F. Coheur, M. De Mazière, I. De Smedt, H.P. Dorn, T. Emmerichs, H. Fuchs, G. Gkatzelis, D.W.T. Griffith, S. Gromov, J.W. Hannigan, F. Hase, T. Hohaus, N. Jones, A. Kerkweg, A. Kiendler-Scharr, E. Lutsch, E. Mahieu, A. Novelli, I. Ortega, C. Paton-Walsh, M. Pommier, A. Pozzer, D. Reimer, S. Rosanka, R. Sander, M. Schneider, K. Strong, R. Tillmann, M. Van Roozendael, L. Vereecken, C. Vigouroux, A. Wahner, D. Taraborrelli, Ubiquitous atmospheric production of organic acids mediated by cloud droplets, Nature. 593 (2021) 233–237.

[10] J. de Gouw, D. Farmer, How ant acid forms in the atmosphere, Nature. 593 (2021) 198–199.

[11]   C.L. Heald, A.H. Goldstein, J.D. Allan, A.C. Aiken, E. Apel, E.L. Atlas, A.K. Baker, T.S. Bates, A.J. Beyersdorf, D.R. Blake, T. Campos, H. Coe, J.D. Crounse, P.F. DeCarlo, J.A. De Gouw, E.J. Dunlea, F.M. Flocke, A. Fried, P. Goldan, R.J. Griffin, S.C. Herndon, J.S. Holloway, R. Holzinger, J.L. Jimenez, W. Junkermann, W.C. Kuster, A.C. Lewis, S. Meinardi, D.B. Millet, T. Onasch, A. Polidori, P.K. Quinn, D.D. Riemer, J.M. Roberts, D. Salcedo, B. Sive, A.L. Swanson, R. Talbot, C. Warneke, R.J. Weber, P. Weibring, P.O. Wennberg, D.R. Worsnop, A.E. Wittig, R. Zhang, J. Zheng, W. Zheng, Total observed organic carbon (TOOC) in the atmosphere: A synthesis of North American observations, Atmos. Chem. Phys. 8 (2008) 2007–2025.

[12]   S.R. Fulgham, D.B. Millet, H.D. Alwe, A.H. Goldstein, S. Schobesberger, D.K. Farmer, Surface Wetness as an Unexpected Control on Forest Exchange of Volatile Organic Acids, Geophys. Res. Lett. 47 (2020) e2020GL088745.

[13]   M.F. Link, T.B. Nguyen, K. Bates, J.F. Müller, D.K. Farmer, Can Isoprene Oxidation Explain High Concentrations of Atmospheric Formic and Acetic Acid over Forests?, ACS Earth Sp. Chem. 4 (2020) 730–740.

[14]   P. Khare, N. Kumar, K.M. Kumari, S.S. Srivastava, Atmospheric Formic and Acetic Acids: An Overview, Rev. Geophys. 37 (1999) 227–248.

[15]   D.B. Millet, M. Baasandorj, D.K. Farmer, J.A. Thornton, K. Baumann, P. Brophy, S. Chaliyakunnel, J.A. De Gouw, M. Graus, L. Hu, A. Koss, B.H. Lee, F.D. Lopez-Hilfiker, J.A. Neuman, F. Paulot, J. Peischl, I.B. Pollack, T.B. Ryerson, C. Warneke, B.J. Williams, J. Xu, A large and ubiquitous source of atmospheric formic acid, Atmos. Chem. Phys. 15 (2015) 6283–6304.

[16]   F. Paulot, D. Wunch, J.D. Crounse, G.C. Toon, D.B. Millet, P.F. Decarlo, C. Vigouroux, N.M. Deutscher, G.G. Abad, J. Notholt, T. Warneke, J.W. Hannigan, C. Warneke, J.A. De Gouw, E.J. Dunlea, M. De Mazière, D.W.T. Griffith, P. Bernath, J.L. Jimenez, P.O. Wennberg, Importance of secondary sources in the atmospheric budgets of formic and acetic acids, Atmos. Chem. Phys. 11 (2011) 1989–2013.

[17]   W.C. Keene, J.N. Galloway, Considerations regarding sources for formic and acetic acids in the troposphere, J. Geophys. Res. 91 (1986) 14466–14474.

[18]   M.F. Shaw, B. Sztáray, L.K. Whalley, D.E. Heard, D.B. Millet, M.J.T. Jordan, D.L. Osborn, S.H. Kable, Photo-tautomerization of acetaldehyde as a photochemical source of formic acid in the troposphere, Nat. Commun. 9 (2018) 2584. http://dx.doi.org/10.1038/s41467-018-04824-2.

[19]   R.W. Talbot, K.M. Beecher, R.C. Harriss, W.R. Cofer, Atmospheric geochemistry of

formic and acetic acids at a mid- latitude temperate site, J. Geophys. Res. 93 (1988) 1638–1652.

[20] P.R. Veres, J.M. Roberts, A.K. Cochran, J.B. Gilman, W.C. Kuster, J.S. Holloway, M. Graus, J. Flynn, B. Lefer, C. Warneke, J. De Gouw, Evidence of rapid production of organic acids in an urban air mass, Geophys. Res. Lett. 38 (2011) L17807.

[21] H.A. Khwaja, Atmospheric concentrations of carboxylic acids and related compounds at a semiurban site, Atmos. Environ. 29 (1995) 127–139.

[22] X. Chen, D.B. Millet, J.A. Neuman, P.R. Veres, E.A. Ray, R. Commane, B.C. Daube, K. McKain, J.P. Schwarz, J.M. Katich, K.D. Froyd, G.P. Schill, M.J. Kim, J.D. Crounse, H.M. Allen, E.C. Apel, R.S. Hornbrook, D.R. Blake, B.A. Nault, P. Campuzano-Jost, J.L. Jimenez, J.E. Dibb, HCOOH in the Remote Atmosphere: Constraints from Atmospheric Tomography (ATom) Airborne Observations, ACS Earth Sp. Chem. 5 (2021) 1436–1454.

[23] B. Yuan, P.R. Veres, C. Warneke, J.M. Roberts, J.B. Gilman, A. Koss, P.M. Edwards, M. Graus, W.C. Kuster, S.M. Li, R.J. Wild, S.S. Brown, W.P. Dubé, B.M. Lerner, E.J. Williams, J.E. Johnson, P.K. Quinn, T.S. Bates, B. Lefer, P.L. Hayes, J.L. Jimenez, R.J. Weber, R. Zamora, B. Ervens, D.B. Millet, B. Rappenglück, J.A. De Gouw, Investigation of secondary formation of formic acid: Urban environment vs. oil and gas producing region, Atom. Chem. Phys. 15 (2015) 1975–1993.

[24] H. Puxbaum, C. Rosenberg, M. Gregori, C. Lanzerstorfer, E. Ober, W. Winiwarter, Atmospheric concentrations of formic and acetic acid and related compounds in eastern and northern Austria, Atmos. Environ. 22 (1988) 2841–2850.

[25] S.K. Akagi, R.J. Yokelson, C. Wiedinmyer, M.J. Alvarado, J.S. Reid, T. Karl, J.D. Crounse, P.O. Wennberg, Emission factors for open and domestic biomass burning for use in atmospheric models, Atmos. Chem. Phys. 11 (2011) 4039–4072.

[26] S. Leach, M. Schwell, D. Talbi, G. Berthier, K. Hottmann, H.W. Jochims, H. Baumgärtel, He I photoelectron spectroscopy of four isotopologues of formic acid: HCOOH, HCOOD, DCOOH and DCOOD, Chem. Phys. 286 (2003) 15–43.

[27] I. Watanabe, Y. Yokoyama, S. Ikeda, Vibrational Structures in the Photoelectron Spectrum of Formic Acid, Chem. Phys. Lett. 19 (1973) 406–409.

[28] M. Suto, X. Wang, L.C. Lee, Fluorescence yields from photodissociative excitation of HCOOH, HCOOCH3, and CH3COOH in the vacuum-ultraviolet region, J. Phys. Chem. 92 (1988) 3764–3768.

[29] W.C. Price, W.M. Evans, The Absorption Spectrum of Formic Acid in the Vacuum

Ultra-Violet, Proc. Roy. Soc. London. 162 (1937) 110–120.

[30] T.L. Ng, S. Bell, The $\pi^* \leftarrow n$ transition of formic acid, J. Mol. Spectrosc. 50 (1974) 166–181.

[31] S. Nagakura, K. Kaya, H. Tsubomura, Vacuum ultraviolet absorption spectra and electronic structures of formic acid, acetic acid and ethyl acetate, J. Mol. Spectrosc. 13 (1964) 1–8.

[32] R. Mualem, E. Sominska, V. Kelner, A. Gedanken, The absorption spectrum of formic-acid dimers in the vacuum ultraviolet region, J. Chem. Phys. 97 (1992) 8813–8814.

[33] S. Leach, M. Schwell, F. Dulieu, J.L. Chotin, H.W. Jochims, H. Baumgärtel, Photophysical studies of formic acid in the VUV. Absorption spectrum in the 6-22 eV region, Phys. Chem. Chem. Phys. 4 (2002) 5025–5039.

[34] S. Bell, T.L. Ng, A.D. Walsh, Vacuum ultra-violet spectra of formic and acetic acids, J. Chem. Soc., Faraday Trans. 2. 71 (1975) 393–401.

[35] H. Basch, M.B. Robin, N.A. Kuebler, Electronic spectra of isoelectronic amides, acids, and acyl fluorides, J. Chem. Phys. 49 (1968) 5007–5018.

[36] E.E. Barnes, W.T. Simpson, Correlations among electronic transitions for carbonyl and for carboxyl in the vacuum ultraviolet, J. Chem. Phys. 39 (1963) 670–675.

[37] D.L. Singleton, G. Paraskevopoulos, R.S. Irwin, UV absorption cross-sections of the monomer and dimer of formic acid, J. Photochem. 37 (1987) 209–216.

[38] T. Ebata, A. Fujii, T. Amano, M. Ito, Photodissociation of Formic Acid: Internal State Distribution of OH Fragment, J. Phys. Chem. 91 (1987) 6095–9097.

[39] G.S. Jolly, D.L. Singleton, G. Paraskevopoulos, Direct determination of the quantum yield of OH in the laser photolysis of formic acid at 222 nm, J. Phys. Chem. 91 (1987) 3463–3465.

[40] R.S. Irwin, D.L. Singleton, G. Paraskevopoulos, R. McLaren, Photochemistry of formic acid monomer at 222 nm, Int. J. Chem. Kinet. 26 (1994) 219–225.

[41] K.W. Lee, K.S. Lee, K.H. Jung, H.R. Volpp, The 212.8-nm photodissociation of formic acid: Degenerate four-wave mixing spectroscopy of the nascent OH(X2IIi) radicals, J. Chem. Phys. 117 (2002) 9266–9274.

[42] M. Schwell, F. Dulieu, H.W. Jochims, J.H. Fillion, J.L. Lemaire, H. Baumgärtel, S. Leach, Photophysical studies of formic acid in the vacuum UV: Fragmentation, fluorescence, and ionization in the 6-23 eV photon energy range, J. Phys. Chem. A. 106 (2002) 10908–10918.

[43] D.L. Singleton, G. Paraskevopoulos, R.S. Irwin, Laser Photolysis of Carboxylic Acids

in the Gas Phase. Direct Determination of the OH Quantum Yield at 222 nm, J. Phys. Chem. 94 (1990) 695–699.

[44]   J.E. Bertie, K.H. Michaelian, The Raman spectra of gaseous formic acid -h2 and -d2, J. Chem. Phys. 76 (1982) 886–894.

[45]   K. Tabayashi, J.I. Aoyama, M. Matsui, T. Hino, K. Saito, Dissociative excitation of HCOOH by single-vacuum ultraviolet and two-ultraviolet photon, J. Chem. Phys. 110 (1999) 9547–9554.

[46]   A. Pelc, W. Sailer, P. Scheier, N.J. Mason, T.D. Märk, Low energy electron attachment to formic acid, Eur. Phys. J. D. 20 (2002) 441–444.

[47]   J.E. Bertie, K.H. Michaelian, H.H. Eysel, D. Hager, The Raman-active O-H and O-D stretching vibrations and Raman spectra of gaseous formic acid-d1 and -OD, J. Chem. Phys. 85 (1986) 4779–4789.

[48]   R.C. Millikan, K.S. Pitzee, Infrared spectra and vibrational assignment of monomeric formic acid, J. Chem. Phys. 27 (1957) 1305–1308.

[49]   T. Ari, J.B. Hasted, Electron Energy-Loss Spectra of Acetaldehyde and Formic Acid, Chem. Phys. Lett. 85 (1982) 153–156.

[50]   T. Ari, M.H. Güven, Valence-shell electron energy-loss spectra of formic acid and acetic acid, J. Electron Spectrosc. Relat. Phenom. 106 (2000) 29–35.

[51]   C. Fridh, Electronic Excitation of Formic Acid, J. Chem. Soc., Faraday Trans. 2. 74 (1978) 190–193.

[52]   V. Vizcaino, M. Jelisavcic, J.P. Sullivan, S.J. Buckman, Elastic electron scattering from formic acid (HCOOH): Absolute differential cross-sections, New J. Phys. 8 (2006) 85.

[53]   D.L. Singleton, G. Paraskevopoulos, R.S. Irwin, G.S. Jolly, D.J. Mckenneys, Rate and Mechanism of the Reaction of Hydroxyl Radicals with Formic and Deuterated Formic Acids, J. Am. Chem. Soc. 110 (1988) 7786–7790.

[54]   D. Demoulin, Empirically adjusted ab initio calculations for the valence and rydberg excited states of formic acid, Chem. Phys. 17 (1976) 471–478.

[55]   F. Ioannoni, D.C. Moule, D.J. Cloutier, Laser Spectroscopic and Quantum Chemical Studies of the Lowest Excited States of Formic Acid, J. Phys. Chem. 94 (1990) 2290–2294.

[56]   V.S. Prabhudesai, D. Nandi, A.H. Kelkar, R. Parajuli, E. Krishnakumar, Dissociative electron attachment to formic acid, Chem. Phys. Lett. 405 (2005) 172–176.

[57]   A. Pelc, W. Sailer, P. Scheier, M. Probst, N.J. Mason, E. Illenberger, T.D. Märk,

22

Dissociative electron attachment to formic acid (HCOOH), Chem. Phys. Lett.. 361 (2002) 277–284.

[58] M. Allan, Study of resonances in formic acid by means of vibrational excitation by slow electrons, J. Phys. B At. Mol. Opt. Phys. 39 (2006) 2939–2947.

[59] M.H.F. Bettega, Low-energy electron collisions with formic acid, Phys. Rev. A. 74 (2006) 054701. https://doi.org/10.1103/PhysRevA.74.054701.

[60] P.A.S. Randi, G.M. Moreira, M.H.F. Bettega, Electron collisions with formic acid, Eur. Phys. J. D. 75 (2021) 306.

[61] T. Yanai, D.P. Tew, N.C. Handy, A new hybrid exchange-correlation functional using the Coulomb-attenuating method (CAM-B3LYP), Chem. Phys. Lett. 393 (2004) 51–57.

[62] G.M.J. Barca, C. Bertoni, L. Carrington, D. Datta, N. De Silva, J.E. Deustua, D.G. Fedorov, J.R. Gour, A.O. Gunina, E. Guidez, T. Harville, S. Irle, J. Ivanic, K. Kowalski, S.S. Leang, H. Li, W. Li, J.J. Lutz, I. Magoulas, J. Mato, V. Mironov, H. Nakata, B.Q. Pham, P. Piecuch, D. Poole, S.R. Pruitt, A.P. Rendell, L.B. Roskop, K. Ruedenberg, T. Sattasathuchana, M.W. Schmidt, J. Shen, L. Slipchenko, M. Sosonkina, V. Sundriyal, A. Tiwari, J.L. Galvez Vallejo, B. Westheimer, M. Włoch, P. Xu, F. Zahariev, M.S. Gordon, Recent developments in the general atomic and molecular electronic structure system, J. Chem. Phys. 152 (2020) 154102.

[63] R. Bauernschmitt, R. Ahlrichs, Treatment of electronic excitations within the adiabatic approximation of time dependent density functional theory., Chem. Phys. Lett. 256 (1996) 454–464.

[64] M.E. Casida, Time-dependent density-functional theory for molecules and molecular solids, J. Mol. Struct.-Theochem. 914 (2009) 3–18.

[65] K. Emrich, An extension of the coupled cluster formalism to excited states (I), Nucl. Phys. A351 (1981) 379–396.

[66] H. Sekino, R.J. Bartlett, A linear response, coupled-cluster theory for excitation energy, Int. J. Quantum Chem. 26 (1984) 255–265.

[67] J.F. Stanton, R.J. Bartlett, The equation of motion coupled-cluster method. A systematic biorthogonal approach to molecular excitation energies, transition probabilities, and excited state properties, J. Chem. Phys. 98 (1993) 7029–7039.

[68] R.J. Bartlett, Coupled-cluster theory and its equation-of-motion extensions, Wiley Interdiscip. Rev. Comput. Mol. Sci. 2 (2012) 126–138.

[69] R.M. Parrish, L.A. Burns, D.G.A. Smith, A.C. Simmonett, A.E. DePrince, E.G.

Hohenstein, U. Bozkaya, A.Y. Sokolov, R. Di Remigio, R.M. Richard, J.F. Gonthier, A.M. James, H.R. McAlexander, A. Kumar, M. Saitow, X. Wang, B.P. Pritchard, P. Verma, H.F. Schaefer, K. Patkowski, R.A. King, E.F. Valeev, F.A. Evangelista, J.M. Turney, T.D. Crawford, C.D. Sherrill, Psi4 1.1: An Open-Source Electronic Structure Program Emphasizing Automation, Advanced Libraries, and Interoperability, J. Chem. Theory Comput. 13 (2017) 3185–3197.

[70] S. Eden, P. Limão-Vieira, S. V. Hoffmann, N.J. Mason, VUV photoabsorption in CF3X (X = Cl, Br, I) fluoro-alkanes, Chem. Phys. 323 (2006) 313–333.

[71] M.H. Palmer, T. Ridley, S.V. Hoffmann, N.C. Jones, M. Coreno, M. De Simone, C. Grazioli, M. Biczysko, A. Baiardi, P. Limão-Vieira, Interpretation of the vacuum ultraviolet photoabsorption spectrum of iodobenzene by ab initio computations, J. Chem. Phys. 142 (2015) 134302.

[72] M.B. Robin, Higher Excited States of Polyatomic Molecules, Volume II, Academic Press, 1975.

[73] S. Iwata, K. Morokuma, Molecular orbital studies of hydrogen chloride, J. Phys. B At. Mol. Phys. 44 (1977) 323–339.

[74] Chemical Kinetics and Photochemical Data for Use in Stratospheric Modelling, Evaluation number 12, NASA, Jet Propulsion Laboratory, JPL, Publication 97-4, January 15, 1997.

[75] P. Limão Vieira, S. Eden, P.A. Kendall, N.J. Mason, S.V. Hoffmann, VUV photo-absorption cross-section for CCl_2F_2, Chem. Phys. Lett. 364 (2002). https://doi.org/10.1016/S0009-2614(02)01304-0.

[76] P.H. Wine, R.J. Astalos, R.L. Mauldin, Kinetic and Mechanistic Study of the OH + HCOOH Reaction, J. Phys. Chem. 89 (1985) 2620–2624.

Figure captions

Fig. 1. The present high-resolution VUV photoabsorption spectrum of HCOOH in the 4.5–10.8 eV photon energy range. See text for details.

Fig. 2. Detail of the VUV photoabsorption spectrum of HCOOH in the 4.5–7.0 eV photon energy range. The 0^0_0 transition is visible in ref. [55] but not in the present work. See text for details.

Fig. 3. Detail of the VUV photoabsorption spectrum of HCOOH in the 7.6–9.4 eV photon energy range. See text for details.

Fig. 4. Detail of the VUV photoabsorption spectrum of HCOOH in the 8.7–10.8 eV photon energy range. See text for details.

Fig. 5. PECs for the nine lowest-lying excited singlet states of the HCOOH *trans*-conformer plotted as a function of the $R_{C=O}$ coordinate (in a_0 units). The calculations were performed at the TD-DFT/CAMB3LYP/aug-cc-pVDZ level of theory in the C_1 symmetry group. See text for details.

Table captions

Table 1. The calculated vertical excitation energies (TD-DFT/CAMB3LYP/aug-cc-pVDZ) and oscillator strengths of the HCOOH *trans*-conformer compared, where possible, with present experimental data. Energies in eV. See text for details.

Table 2a. Proposed vibrational assignments of the HCOOH *trans*-conformer absorption band in the photon energy range 4.5−7.0 eV[a]. Energies in eV. See text for details.

Table 2b. Proposed vibrational assignments for progressions of the HCOOH *trans*-conformer absorption band in the photon energy range 4.5−7.0 eV[a]. Energies in eV. See text for details

Table 3. Proposed vibrational assignments of the HCOOH *trans*-conformer absorption bands in the photon energy range 7.6−9.4 eV[a]. Energies in eV. See text for details

25

Table 5. Energy values (eV), quantum defects (δ) and assignments of the Rydberg series converging to the ionic electronic ground $(10a')^{-1}$ state and the first ionic electronic excited state $(2a'')^{-1}$ of formic acid, HCOOH. See text for details.

Table 6. Proposed vibrational assignments of HCOOH *trans*-conformer Rydberg series converging to the ionic electronic ground state $(10a')^{-1}$ in the photon energy range 8.7−10.8 eV[a]. Energies in eV. See text for details.

Table 7. Proposed vibrational assignments of HCOOH *trans*-conformer Rydberg series converging to the ionic electronic first excited state $(2a'')^{-1}$ in the photon energy range 8.7−10.8 eV[a]. Energies in eV. See text for details

Fig. 1. The present high-resolution VUV photoabsorption spectrum of HCOOH in the 4.5–10.8 eV photon energy range. See text for details.

Fig. 2. Details of the VUV photoabsorption spectrum of HCOOH in the 4.5–7.0 eV photon energy range. The 0_0^0 transition is visible in ref. [55] but not in the present work. See text for details.

28

Fig. 3. Detail of the VUV photoabsorption spectrum of HCOOH in the 7.6–9.4 eV photon energy range. See text for details.

Fig. 4. Detail of the VUV photoabsorption spectrum of HCOOH in the 8.7–10.8 eV photon energy range. See text for details.

Fig. 5. PECs for the nine lowest-lying excited singlet states of the HCOOH *trans*-conformer plotted as a function of the $R_{C=O}$ coordinate (in a_0 units). The calculations were performed at the TD-DFT/CAMB3LYP/aug-cc-pVDZ level of theory in the C_1 symmetry group. See text for details.

31

Table 1. The calculated vertical excitation energies (TD-DFT/CAMB3LYP/aug-cc-pVDZ) and oscillator strengths of the HCOOH *trans*-conformer compared, where possible, with the present experimental data. Energies in eV. See text for details.

trans-conformer				Assignment	E (eV) expt.[a]	Cross-section (Mb)
State	E (eV)	f_L	Dominant excitations			
$\tilde{X}\,^1A'$						
$1\,^1A''$	5.767	0.000930	$3a'' \leftarrow 10a'$	$\pi^* \leftarrow \bar{n}_O$	5.910	0.19
$2\,^1A'$	7.542	0.026277	$3a'' \leftarrow 2a''$; $11a' \leftarrow 10a'$	$\pi^* \leftarrow \pi_{C=O}$; $3s \leftarrow \bar{n}_O$	7.51(4)	5.22
$3\,^1A'$	8.066	0.045708	$15a' \leftarrow 10a'$; $12a' \leftarrow 10a'$	$3s \leftarrow \bar{n}_O$; $3s \leftarrow \bar{n}_O$	8.109	25.39
$2\,^1A''$	8.293	0.002934	$11a' \leftarrow 2a''$			
$4\,^1A'$	8.573	0.152206	$11a' \leftarrow 10a'$; $13a' \leftarrow 10a'$; $3a'' \leftarrow 2a''$	$3s \leftarrow \bar{n}_O$; $3p \leftarrow \bar{n}_O$; $\pi^* \leftarrow \pi_{C=O}$	8.285	35.13
$5\,^1A'$	9.070	0.097632	$11a' \leftarrow 10a'$; $13a' \leftarrow 10a'$	$\sigma^* \leftarrow \bar{n}_O$	8.952	35.97
$3\,^1A''$	9.072	0.097632	$4a'' \leftarrow 10a'$			
$4\,^1A''$	9.200	0.002003	$15a' \leftarrow 2a''$; $12a' \leftarrow 2a''$	$3s \leftarrow \pi_{C=O}$	8.923	28.43
$5\,^1A''$	9.330	0.000121	$4a'' \leftarrow 9a'$; $3a'' \leftarrow 9a'$			
$6\,^1A'$	9.969	0.024875	$14a' \leftarrow 10a'$	$4s \leftarrow \bar{n}_O$	9.995	15.52
$6\,^1A''$	10.072	0.045796	$13a' \leftarrow 2a''$	$3p \leftarrow \pi_{C=O}$	9.947	20.40
$7\,^1A'$	10.165	0.019211	$3a'' \leftarrow 2a''$; $4a'' \leftarrow 2a''$			
$8\,^1A'$	10.509	0.043079	$16a' \leftarrow 10a'$; $11a' \leftarrow 9a'$			
$9\,^1A'$	10.745	0.023103	$19a' \leftarrow 10a'$; $18a' \leftarrow 10a'$; $15a' \leftarrow 10a'$	$5d \leftarrow \bar{n}_O$	10.749	13.06
$10\,^1A'$	10.848	0.007063	$11a' \leftarrow 9a'$; $16a' \leftarrow 10a'$; $17a' \leftarrow 10a'$			
$6\,^1A''$	10.884	0.000283	$14a' \leftarrow 2a''$			

[a] the last decimal of the energy value is given in brackets for these less-resolved features;
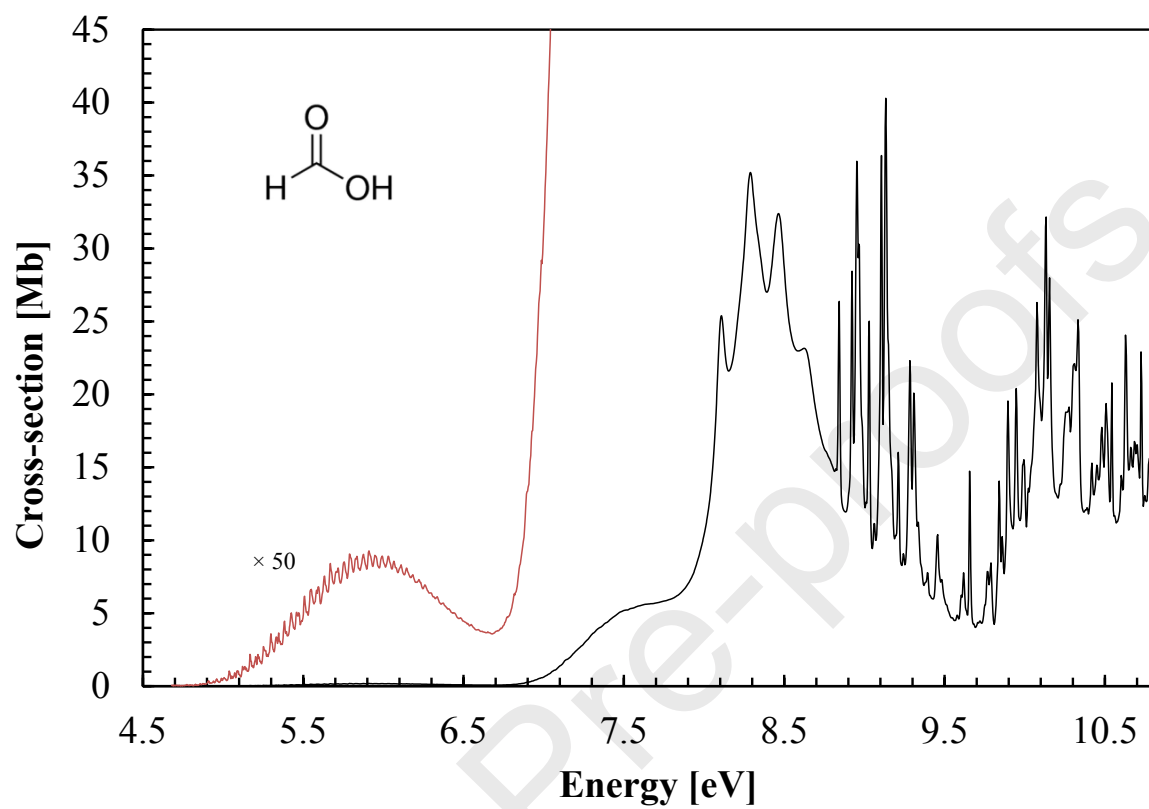
Table 2a. Proposed vibrational assignments of the HCOOH *trans*-conformer absorption band in the photon energy range 4.5−7.0 eV[a]. Energies in eV. See text for details.

	This work					Previous work
assignment	energy	$\Delta E\,(\upsilon_3')$	$\Delta E\,(\upsilon_7')$	$\Delta E\,(\upsilon_8')$	$\Delta E\,(\upsilon_9')$	ref. [30]
$\pi_{CO}^*(3a'')\leftarrow n_O(10a'),\,\left(1^1A''\leftarrow\tilde{X}^1A'\right)$						
0_0^0	(4.641)[55]	…	–	–	–	–
3_0^1	4.772	0.131	–	–	–	4.776
$3_0^1 + 7_0^1$	4.82(6)(w)	–	0.054	–	–	–
$3_0^1 + 7_0^2 / 3_0^1 + 8_0^1$	4.87(9)(w)	–	0.053	0.107	–	–
3_0^2	4.89(3)(s)	0.121	–	–	–	4.910
$3_0^2 + 7_0^1$	4.938	–	0.045	–	–	–
$3_0^2 + 7_0^2 / 3_0^2 + 8_0^1$	4.99(3)(s,w)	–	0.055	0.100	–	–
3_0^3	5.00(3)(s)	0.110	–	–	–	5.041
$3_0^3 + 7_0^1$	5.05(7)(s)	–	0.054	–	–	–
$3_0^3 + 7_0^2 / 3_0^3 + 8_0^1$	5.10(4)(s)	–	0.047	0.101	–	–
3_0^4	5.136	0.133	–	–	–	5.170
$3_0^4 + 9_0^1$	5.168	–	–	–	0.032	–
$3_0^4 + 7_0^1$	5.179	–	0.043	–	–	–
$3_0^4 + 9_0^2$	5.203	–	–	–	0.035	–
$3_0^4 + 7_0^1 + 9_0^1$	5.216	–	–	–	0.037	–
$3_0^4 + 7_0^2 / 3_0^4 + 8_0^1$	5.225	–	0.046	0.089	–	–
$3_0^4 + 7_0^1 + 9_0^2$	5.254	–	–	–	0.038	–
3_0^5	5.26(0)(s)	0.124	–	–	–	5.300
$3_0^5 + 7_0^1 + 9_0^1$	5.299	–	–	–	0.039	–
$3_0^5 + 7_0^1$	5.30(8)(s)	–	0.048	–	–	–
$3_0^5 + 7_0^1 + 9_0^2$	5.333	–	–	–	0.034	–
$3_0^5 + 7_0^2 / 3_0^5 + 8_0^1$	5.347	–	0.039	0.087	–	–
3_0^6	5.384	0.124	–	–	–	5.428
$3_0^6 + 7_0^1$	5.43(3)(s)	–	0.049	–	–	–
$3_0^6 + 7_0^2 / 3_0^6 + 8_0^1$	5.472	–	0.039	0.088	–	–
3_0^7	5.508	0.124	–	–	–	5.552
$3_0^7 + 7_0^1$	5.550	–	0.042	–	–	–
$3_0^7 + 7_0^2 / 3_0^7 + 8_0^1$	5.593	–	0.043	0.085	–	–
3_0^8	5.631	0.123	–	–	–	5.670
$3_0^8 + 9_0^1$	5.669	–	–	–	0.038	–
$3_0^8 + 7_0^1$	5.67(7)(s)	–	0.046	–	–	–

$3_0^8 + 9_0^2$	5.703	–	–	–	0.034	–
$3_0^8 + 7_0^2 / 3_0^8 + 8_0^1$	5.719	–	0.042	0.088	–	–
3_0^9	5.753	0.122	–	–	–	5.792
$3_0^8 + 7_0^2 + 9_0^1$	5.756	–	–	–	0.037	–
$3_0^8 + 7_0^2 + 9_0^2$	5.791	–	–	–	0.035	–
$3_0^9 + 7_0^1$	5.79(9)(s)	–	0.046	–	–	–
$3_0^9 + 7_0^1 + 9_0^1$	5.835	–	–	–	0.036	–
$3_0^9 + 7_0^2 / 3_0^9 + 8_0^1$	5.851	–	0.052	0.098	–	–
$3_0^9 + 7_0^1 + 9_0^2$	5.86(5)(s)	–	–	–	0.030	–
3_0^{10}	5.876	0.123	–	–	–	5.910
$3_0^{10} + 9_0^1$	5.910	–	–	–	0.034	–
$3_0^{10} + 7_0^1$	5.92(1)(s)	–	0.045	–	–	–
$3_0^{10} + 7_0^2 / 3_0^{10} + 8_0^1$	5.96(9)(s)	–	0.048	0.093	–	–
3_0^{11}	5.993	0.117	–	–	–	6.032
$3_0^{11} + 7_0^1$	6.03(9)(s)	–	0.046	–	–	–
$3_0^{11} + 7_0^2$	6.08(1)(s)	–	0.042	0.088	–	–
3_0^{12}	6.111	0.118	–	–	–	6.145
$3_0^{12} + 9_0^1$	6.147	–	–	–	0.036	–
$3_0^{12} + 7_0^1$	6.15(3)(s)	–	0.042	–	–	–
$3_0^{12} + 9_0^2$	6.18(1)(s)	–	–	–	0.034	–
$3_0^{12} + 7_0^2 / 3_0^{12} + 8_0^1$	6.21(2)(w)	–	0.059	0.101	–	–
3_0^{13}	6.23(4)(s)	0.123	–	–	–	6.261
$3_0^{13} + 9_0^1$	6.262	–	–	–	0.028	–
$3_0^{13} + 7_0^1$	6.27(7)(s)	–	0.043	–	–	–
$3_0^{13} + 9_0^2$	6.28(7)(w)	–	–	–	0.025	–
$3_0^{13} + 7_0^2 / 3_0^{13} + 8_0^1$	6.31(9)(s)	–	0.042	0.085	–	–
3_0^{14}	6.35(5)(s,w)	0.121	–	–	–	–
$3_0^{14} + 7_0^1$	6.401	–	0.046	–	–	–
$3_0^{14} + 7_0^2 / 3_0^{14} + 8_0^1$	6.45(1)(s)	–	0.050	0.096	–	–
3_0^{15}	6.478	0.123	–	–	–	–
$3_0^{15} + 9_0^1$	6.51(5)(s,w)	–	–	–	0.037	–
$3_0^{15} + 7_0^1$	6.51(9)(w)	–	0.041	–	–	–
$3_0^{15} + 9_0^2$	6.550	–	–	–	0.035	–
$3_0^{15} + 7_0^2 / 3_0^{15} + 8_0^1$	6.57(0)(s,w)	–	0.051	0.092	–	–
$\overline{\Delta E}$		0.123	0.047	0.093	0.034	

[a] (w) weak feature; (s) shoulder structure (the last decimal of the energy value is given in brackets for these less-resolved features);

Table 2b. Proposed vibrational assignments for progressions of the HCOOH *trans*-conformer absorption band in the photon energy range 4.5−7.0 eV[a]. Energies in eV. See text for details.

assignment	Energy	$\Delta E\,(\upsilon_3')$	assignment	energy	$\Delta E\,(\upsilon_3')$	$\Delta E\,(\upsilon_9')$
$\pi^*_{CO}(3a'')\leftarrow n_O(10a'),\,(1^1A''\leftarrow \tilde{X}^1A')$						
3^n	4.83(0)(w)	…	…	…	…	…
3^{n+1}	4.95(6)(w)	0.126	3^n	4.95(7)(w)	…	…
3^{n+2}	5.071	0.115	3^{n+1}	5.09(0)(w)	0.133	…
3^{n+3}	5.19(9)(s)	0.128	3^{n+2}	5.203	0.113	…
3^{n+4}	5.31(4)(w)	0.115	3^{n+3}	5.333	0.130	…
3^{n+5}	5.43(3)(s)	0.119	3^{n+4}	5.457	0.124	…
3^{n+6}	5.550	0.117	$3^{n+4}+9_0^1$	5.48(9)(s)	…	0.032
3^{n+7}	5.670	0.120	$3^{n+4}+9_0^2$	5.52(5)(s)	…	0.036
3^{n+8}	5.791	0.121	3^{n+5}	5.590	0.133	…
3^{n+9}	5.910	0.119	3^{n+6}	5.703	0.113	…
3^{n+10}	6.030	0.120	3^{n+7}	5.829	0.126	…
3^{n+11}	6.147	0.117	3^{n+8}	5.952	0.123	…
3^{n+12}	6.262	0.115	3^{n+9}	6.066	0.114	…
3^{n+13}	6.375	0.113	3^{n+10}	6.184	0.118	…
3^{n+14}	6.48(5)(s)	0.110	3^{n+11}	6.31(9)(b)	0.135	…
…	…	…	3^{n+12}	6.43(1)(b)	0.112	…
…	…	…	3^{n+13}	6.56(7)(s)	0.136	…

[a] (w) weak feature; (s) shoulder structure; (b) broad structure; (the last decimal of the energy value is given in brackets for these less-resolved features);

35

Table 3. Proposed vibrational assignments of the HCOOH *trans*-conformer absorption bands in the photon energy range 7.6−9.4 eV[a]. Energies in eV. See text for details.

assignment	energy	$\Delta E\ (\upsilon_3')$	$\Delta E\ (\upsilon_5')$	$\Delta E\ (\upsilon_7')$	ref. [33]
	This work				Previous work
$\pi^*(3a'')\leftarrow\pi_{C=O}(2a''),\ (4^1A'\leftarrow\tilde{X}^1A')$					
0_0^0	8.109	…	…	…	8.106
3_0^1	8.285	0.176	…	…	8.290
$3_0^1 + 7_0^1$	8.34(1)(s,w)	…	…	0.056	…
3_0^2	8.466	0.181	…	…	8.460
3_0^3	8.62(8)(s,b)	0.162	…	…	…
$3_0^3 + 5_0^1$	8.77(1)(s,w)	…	0.143	…	…
3_0^4	8.82(1)(w)	0.193	…	…	…
3_0^5	9.01(7)(w)	0.196	…	…	…
3_0^6	9.20(1)(w)	0.184	…	…	…

[a] (s) shoulder structure; (w) weak feature; (b) broad structure (the last decimal of the energy value is given in brackets for these less-resolved features);

Table 4. Proposed vibrational assignments of the HCOOH *trans*-conformer absorption bands in the photon energy range 8.7−10.8 eV[a]. Energies in eV. See text for details.

assignment	energy	ΔE (υ_3')	ΔE (υ_6')	ΔE (υ_7')	ref. [33]
	This work				Previous work
$3s(12a')\leftarrow\pi_{C=O}(2a''),\ (4^1A''\leftarrow\tilde{X}^1A')$					
0_0^0	8.923	…	…	…	8.918
7_0^1	8.98(4)(s)	…	…	0.061	8.96
6_0^1	9.01(7)(w)	…	0.094	…	…
3_0^1	9.106	0.183	…	…	9.103
$3_0^1 + 7_0^1$	9.17(0)(s)	…	…	0.064	9.147
$3_0^1 + 6_0^1$	9.20(1)(s,w)	…	0.095	…	…
3_0^2	9.284	0.178	…	…	9.28
$3_0^2 + 7_0^1$	9.35(4)(s)	…	…	0.070	9.33
$3_0^2 + 6_0^1$	9.37(8)(s,w)	…	0.094	…	…
3_0^3	9.457	0.173	…	…	9.45
$3_0^3 + 7_0^1$	9.53(0)(s,w)	…	…	0.073	9.50
$3_0^3 + 6_0^1$	9.54(1)(s,w)	…	0.084	…	…
3_0^4	9.619	0.162	…	…	9.613
$3_0^4 + 7_0^1$	9.68(6)(s,w)	…	…	0.067	…
$3_0^4 + 6_0^1$	9.70(9)(s,w)	…	0.090	…	…
3_0^5	9.790	0.171	…	…	9.782
$\sigma^*\leftarrow\overline{n}_O(10a'),\ (5^1A'\leftarrow\tilde{X}^1A')$					
0_0^0	8.952	…	…	…	8.95
7_0^1	9.01(7)(w)	…	…	0.065	…
3_0^1	9.133	0.181	…	…	9.13
$3_0^1 + 7_0^1$	9.19(4)(s,w)	…	…	0.061	…
3_0^2	9.308	0.175	…	…	9.306
3_0^3	9.483	0.175	…	…	9.478
$3_0^3 + 7_0^1$	9.54(8)(s,w)	…	…	0.065	…

[a] (s) shoulder structure; (w) weak feature (the last decimal of the energy value is given in brackets for these less-resolved features);

Table 5. Energy values (eV), quantum defects (δ) and assignments of the Rydberg series converging to the ionic electronic ground $(10a')^{-1}$ state and the first ionic electronic excited state $(2a'')^{-1}$ of formic acid, HCOOH. See text for details.

trans-conformer				
	This work		Ref. [33]	Ref. [34]
E_n	δ	assignment	E_n	E_n
IE$_1$ = 11.3246 eV $(10a')^{-1}$				
(*nsa'* ← *10a'*)				
7.51(4)(b)/8.109	1.11/0.94	3sa'	7.533	8.105
9.995	0.80	4sa'	9.987	9.946
10.543	0.83	5sa'	10.533	10.539
(*npa'* ← *10a'*)				
8.843	0.66	3pa'	8.839	8.951
10.154	0.59	4pa'	10.147	10.511
10.629	0.58	5pa'	10.621	10.628
(*np'a'* ← *10a'*)				
9.063	0.55	3p'a'	9.059	–
10.226	0.48	4p'a'	10.375	–
10.661	0.47	5p'a'	–	–
(*nda'* ← *10a'*)				
9.656	0.14	3da'	9.651	9.655
10.419	0.12	4da'	10.410	10.415
10.749	0.14	5da'	10.769	10.770
IE$_2$ = 12.3783 eV $(2a'')^{-1}$				
(*nsa'* ← *2a''*)				
8.923/8.958	1.01/1.00	3sa'	8.761	–
(*npa'* ← *2a''*)				
9.770	0.72	3pa'	9.763	–
(*npa''* ← *2a''*)				
9.947	0.63	3pa''	9.942	–
(*nda''* ← *2a''*)				
10.725	0.13	3da''	10.717	–

[a] (b) broad structure; (w) weak feature; (s) shoulder structure (the last decimal of the energy value is given in brackets for these less-resolved features);

Table 6. Proposed vibrational assignments of HCOOH *trans*-conformer Rydberg series converging to the ionic electronic ground state $(10a')^{-1}$ in the photon energy range 8.7−10.8 eV[a]. Energies in eV. See text for details.

assignment	energy	ΔE (υ_3')	ΔE (υ_5')	ΔE (υ_6')	ΔE (υ_7')	ref. [33]
		This work				Previous work
$(3pa' \leftarrow 10a')$	8.843	–	–	–	–	8.839
7_0^1	8.90(1)(s)	–	–	–	0.058	–
5_0^1	8.98(4)(s)	–	0.141	–	–	8.983
3_0^1	9.030	0.187	–	–	–	9.026
$3_0^1 + 5_0^1$	9.17(0)(s)	–	0.140	–	–	9.165
3_0^2	9.211	0.181	–	–	–	9.209
$3_0^2 + 5_0^1$	9.35(4)(s)	–	0.143	–	–	9.356
3_0^3	9.393	0.182	–	–	–	9.390
$3_0^3 + 5_0^1$	9.53(0)(s,w)	–	0.137	–	–	–
3_0^4	9.57(8)(b,w)	0.185	–	–	–	–
$3_0^4 + 5_0^1$	9.720	–	0.142	–	–	–
$3_0^4 + 5_0^2$	9.860	–	0.140	–	–	–
$(3p'a' \leftarrow 10a')$	9.063	–	–	–	–	9.059
5_0^1	9.211	–	0.148	–	–	–
3_0^1	9.242	0.179	–	–	–	9.243
$3_0^1 + 5_0^1$	9.393	–	0.151	–	–	–
3_0^2	9.42(5)(w)	0.183	–	–	–	–
$3_0^2 + 5_0^1$	9.57(8)(b,w)	–	0.153	–	–	–
3_0^3	9.604	0.179	–	–	–	–
$3_0^3 + 5_0^1$	9.75(5)(s)	–	0.151	–	–	–
$(3da' \leftarrow 10a')$	9.656	–	–	–	–	9.651
3_0^1	9.840	0.184	–	–	–	9.835
3_0^2	10.023	0.183	–	–	–	10.016
3_0^3	10.19(2)(s,w)	0.169	–	–	–	–
$(4sa' \leftarrow 10a')$	9.995	–	–	–	–	9.987
7_0^1	10.05(6)(s)	–	–	–	0.061	–
$5_0^1/6_0^1$	10.134	–	0.139	0.139	–	10.125
3_0^1	10.17(9)(s)	0.184	–	–	–	10.170

|						
$3_0^1 + 5_0^1/6_0^1$	10.332	–	0.153	0.153	–	–
$(4pa' \leftarrow 10a')$	10.154	–	–	–	–	10.147
$5_0^1/6_0^1$	10.30(2)(b)	–	0.148	0.148	–	10.299
3_0^1	10.332	0.178	–	–	–	10.324
5_0^2	10.450	–	0.148	–	–	10.422
$3_0^1 + 5_0^1/6_0^1$	10.481	–	0.149	0.149	–	10.470
3_0^2	10.507	0.175	–	–	–	10.498
$3_0^2 + 5_0^1/6_0^1$	10.661	–	0.154	0.154	–	10.653
3_0^3	10.684	0.177	–	–	–	–
$(4p'a' \leftarrow 10a')$	10.226	–	–	–	–	10.375
3_0^1	10.38(8)(w)	0.162	–	–	–	–
3_0^2	10.56(1)(s,w)	0.173	–	–	–	–
$(4da' \leftarrow 10a')$	10.419	–	–	–	–	10.410
3_0^1	10.602	0.183	–	–	–	10.595
$(5sa' \leftarrow 10a')$	10.543	–	–	–	–	10.533
7_0^1	10.602	–	–	–	0.059	–
$5_0^1/6_0^1$	10.684	–	0.141	0.141	–	10.684
3_0^1	10.725	0.182	–	–	–	10.717
$(5pa' \leftarrow 10a')$	10.629	–	–	–	–	–
7_0^1	10.684	–	–	–	0.055	–
$(5p'a' \leftarrow 10a')$	10.661	–	–	–	–	–
7_0^1	10.725	–	–	–	0.064	–

[a] (s) shoulder structure; (w) weak feature; (b) broad structure (the last decimal of the energy value is given in brackets for these less-resolved features);

Table 7. Proposed vibrational assignments of HCOOH *trans*-conformer Rydberg series converging to the ionic electronic first excited state $(2a'')^{-1}$ in the photon energy range 8.7−10.8 eV[a]. Energies in eV. See text for details.

| assignment | This work | | | | Previous work |
	energy	$\Delta E\,(\upsilon_3')$	$\Delta E\,(\upsilon_5')$	$\Delta E\,(\upsilon_6')$	ref. [33]
$(3sa' \leftarrow 2a'')$	8.958	−	−	−	8.761
6_0^1	9.063	−	−	0.105	−
3_0^1	9.14(7)(s)	0.189	−	−	−
3_0^2	9.333	0.186	−	−	−
$3_0^2 + 5_0^1$	9.483	−	0.150	−	−
$(3pa' \leftarrow 2a'')$	9.770	−	−	−	9.763
6_0^1	9.860	−	−	0.090	9.891
3_0^1	10.04(3)(s)	0.273	−	−	10.053
3_0^2	10.31(1)(b)	0.268	−	−	−
3_0^3	10.59(2)(s,w)	0.281	−	−	−
$3_0^1 + 5_0^1$	10.702	−	−	0.110	−
$(3pa'' \leftarrow 2a'')$	9.947	−	−	−	9.942
6_0^1	10.076	−	−	0.129	10.071
5_0^1	10.09(6)(s)	−	0.149	−	10.086
3_0^1	10.25(5)(b)	0.308	−	−	10.256

[a] (s) shoulder structure; (w) weak feature; (b) broad structure (the last decimal of the energy value is given in brackets for these less-resolved features);

41

Graphical Abstract
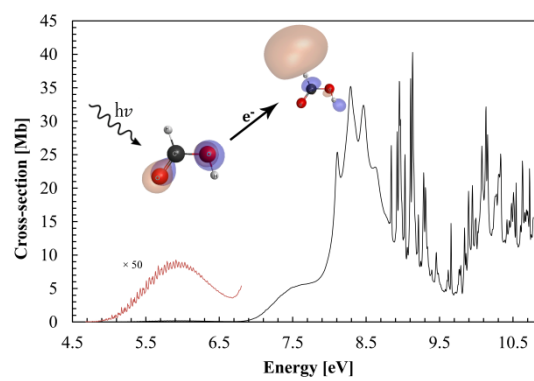
42

Electronically excited states of formic acid investigated by theoretical and experimental methods

P. A. S. Randi [a], D. F. Pastega [a], M. H. F. Bettega [a], N. C. Jones [b],

S. V. Hoffmann [b], S. Eden [c], A. Souza Barbosa [a,*] and P. Limão-Vieira [a,d,*]

Highlights

- Formic acid vacuum ultraviolet photoabsorption spectrum
- Absolute cross-section values in the photon energy range 4.7–10.8 eV
- Electronic state spectroscopy of Rydberg and mixed valence/Rydberg transitions
- Theoretical calculations at time dependent density functional theory level
- Potential energy curves as a function of the C=O coordinate

Author statement

PASR, DFP, ASB and MHFB have performed the quantum chemical calculations; PASR, ASB, PLV wrote the manuscript draft; NCJ, SVH have contributed with the experimental aspects of the synchrotron beam line used for the experiments; MHFB, NCJ, SVH, SE and PLV revised the manuscript.

45

Declaration of interests

☒ The authors declare that they have no known competing financial interests or personal relationships that could have appeared to influence the work reported in this paper.

☐ The authors declare the following financial interests/personal relationships which may be considered as potential competing interests: